Computational Materials Science 108 (2015) 258–263

Contents lists available at ScienceDirect

Computational Materials Science

journal homepage: www.elsevier.com/locate/commatsci

Effect of twin boundaries and structural polytypes on electron transport in GaAs

Xiaofeng Qian [a], Mitsumoto Kawai [b], Hajime Goto [b], Ju Li [a,*]

[a] Department of Nuclear Science and Engineering and Department of Materials Science and Engineering, Massachusetts Institute of Technology, Cambridge, MA 02139, USA
[b] Honda R&D Co., Ltd., 1-4-1 Chuo, Wako-shi, Saitama 351-0193, Japan

ARTICLE INFO

Article history:
Received 11 April 2015
Accepted 5 June 2015
Available online 15 July 2015

Keywords:
GaAs nanowire
Twin boundaries
Structural polytypes
Electron transport
First-principles calculations
Photovoltaics

ABSTRACT

As-grown GaAs nanowires often possess high density of twin boundaries and stacking faults, which serve as scattering planes for electrons. Here, using density functional theory and Green's function method, we demonstrate that the planar faults can significantly alter the transport properties depending on different planar defects and in-plane wavevector of the electronic state. Conductance eigenchannel analysis was applied to reveal the microscopic mechanism of electron scattering. A formalism is developed to estimate the reduction of the electron and hole mobilities due to planar faults and structural polytypes, based on quantum transmission coefficients computed in phase-coherent transport calculations. For twin spacing of 2.4 nm, electron mobility and hole mobility were predicted to be 3000 $cm^2/V/s$ and 500 $cm^2/V/s$, respectively. The findings highlight the necessity of removing twins for high-performance nanowire solar cells.

1. Introduction

One-dimensional nanostructures such as nanowire and nanotube have been extensively studied in the past two decades owing to the low-dimensionality and quantum-confinement induced novel physical and chemical properties [1]. In particular, III–V nanowires such as GaAs are promising platforms for electronic, photonic, and photovoltaic applications [2–5]. However, as-grown III–V nanowires, for example, GaAs and GaP, often possess high density of coherent twin boundaries and alternating cubic zinc blend (ZB) and hexagonal wurtzite (WZ) polytype structures normal to the most favorable growth direction ⟨1 1 1⟩ [6–10]. The ZB structure is a staggered conformation which is sterically more favorable, while the WZ structure is an eclipsed conformation which is electrostatically more favorable. The competition between steric and electrostatic interactions results in a small cohesive energy difference of only 12 meV/atom between the WZ and ZB phases in GaAs, where ZB is thermodynamically more stable [11,12].

Effect of these planar crystalline defects on the physical properties of nanowires have been studied both experimentally [10,13] and theoretically [12,14–18]. In particular, Shimamura et al. predicted that the exciton radiative decay time increases while the electron mobility significantly decreases in the presence of twin boundary in GaAs [17]. However, microscopic understanding of electron scattering near stacking faults and twin boundaries is still lacking, as well as their effect on the mesoscale diffusive transport properties. Thelander et al. stated that although the polytype mixtures of WZ and ZB in InAs nanowire can increase the resistivity by up to 2 orders of magnitude, the stacking faults and twin planes do not appear to have significant impact on the electrical conductivity σ [10]. Since

$$\sigma = e(c_e M_e + c_h M_h), \tag{1}$$

where c_e and M_e is the electron carrier concentration and mobility, respectively, and c_h and M_h is the hole carrier concentration and mobility, respectively. A partial cancelation of c and M trends could mask the individual sensitivity on planar defects. It therefore behooves one to predict the mobility M (relating average carrier drift velocity with applied electric field) from *ab initio* calculations directly.

Recently, phase-coherence length (frequency/energy conservation length) of electrons has been measured to be several hundred nms at low temperature in III–V nanowires even with high density of stacking faults [19–21], while the momentum conservation length – aka the mean-free path (MFP, λ_{MFP}) – tends to be much shorter [19]. The classical Drude model relates mobility M with momentum relaxation time τ:

* Corresponding author. Tel.: +1 617 253 0166; fax: +1 617 258 8863.
E-mail address: liju@mit.edu (J. Li).

http://dx.doi.org/10.1016/j.commatsci.2015.06.011
0927-0256/

$$M = \frac{e\tau}{m^*}, \tag{2}$$

where m^* is the effective mass of the electron/hole carrier. Because (2) is a coarse-grained expression, we need to relate M and τ to the microscopics. Based on a static microscopic structure, phase-coherent transmission coefficient $0 \leqslant T_n \leqslant 1$ can be calculated using *ab initio* methods, where n is the quantum number of the electronic state [22–25]. λ_{MFP}, τ and T_n describe elastic scattering, where electron energy is conserved but momentum is not. But some kind of statistical averaging is needed to connect the two.

In this paper, using first-principles density-functional theory (DFT) [26,27] and Green's function method [22,23], we calculated the electrical conductance in GaAs⟨1 1 1⟩ nanowire without defect and with eight forms of polytypes. Using conductance eigenchannel analysis, we show that T_n highly depends on different polytype, energy, and **k**-point in two-dimensional (2D) Brillouin zone (BZ) due to the quantum-interference effect. In addition, microscopic scattering mechanism near the planar defects is revealed. We then perform averaging over $\{T_n\}$ to obtain M_{e} and M_{h}.

2. Quantum conductance and transmission coefficient

Quantum transport calculations are performed using the Green's function method module [23] in the SIESTA code [28]. We also modified the code to calculate and visualize the conductance eigenchannels [25,29]. In our calculations, we employed the generalized-gradient approximation (GGA) [30,31] of exchange–correlation functionals in the Perdew–Berke–Ernzerhof (PBE) form [32], mesh cutoff of 300 Rydberg, Troullier–Martins pseudopotential [33], and single-ζ basis plus polarization orbitals for pseudo-atomic orbital minimal basis. Although in principle one could build a true nanowire geometry for theoretical investigation, such approach is not only very time-consuming, but also unnecessary considering the fact that the diameter of most GaAs nanowires synthesized is on the order of 100 nm, that is, more than 400 times of Ga-As bond length. In such nanowires, the charge transport will be dominantly through the bulk. Therefore, we approximate the nanowire with the bulk GaAs, having its z axis aligned to the ⟨1 1 1⟩ growth direction. In this case, Monkhorst–Pack **k**-point samplings [34] of $7 \times 7 \times 1$ and $31 \times 31 \times 1$ are applied to the self-consistent electronic structure calculation and electrical conductance calculation, respectively. Current–voltage curve is obtained by integrating the **k**-point- and energy-dependent conductance curve in the zero-bias voltage limit.

Fig. 1(a) shows the simulation setup of phase-coherent quantum transport through GaAs⟨1 1 1⟩ nanowire, which consists of top lead, central device, and bottom lead. In order to understand the impact of stacking faults and twin boundaries, we placed 9 different representative polytype structures in the central device including pristine, 3C, 2H, 4H, 6H, 9R, 15R, 2AB, and 3AB. The detailed sequences are shown in Fig. 1(b).

Fig. 2(a) shows the calculated energy-dependent electrical conductance, $G(E)$, in the unit of quantum conductance $2e^2/h$, where "2" accounts for spin-degeneracy. The Fermi level is located at $E = 0$ eV. For better comparison, we also plot the conductance ratio with respect to the conductance of pristine GaAs nanowire as a function of E, $G/G_{\mathrm{p}}(E)$, in Fig. 2(b). Similarly, we also plot the current–voltage curve $I(V)$ and current ratio $I/I_{\mathrm{p}}(V)$ in Fig. 2(c) and (d). Fig. 2(a) clearly demonstrates that, compared to the pristine GaAs nanowire, the overall conductance has a notable drop for all polytypes, consequently the current also decreases significantly. However, the change is highly energy- and polytype-dependent. Close to valence and conduction band edges, polytype 3AB, 2AB, and 9R have the largest impact on the total conductance and current, while 3C, 2H, 4H, and 6H do not have much effect. Small conductance in the energy gap of Fig. 2(b) is not physical conductance and should be ignored as it is solely due to the Gaussian smearing of conductance. Moving away from the Fermi level, all the polytypes have the similar magnitude of reduction in the conductance, thus the integrated total current approaches to the similar magnitude as well.

To understand the large impact of 3AB, 2AB, and 9R, we carefully inspected the sequences shown in Fig. 1(b), and found a similar structural feature, that is, all three polytypes contain segment of "-ABAB-" WZ structure. The WZ structure has larger band gap than the ZB structure of GaAs, hence the conductance near the valence and conduction edges of the original ZB GaAs nanowire will be affected most, which is indeed what we have observed in Fig. 2(b) and (d).

In order to have a microscopic understanding of electron scattering near the twin boundaries and stacking faults, we have modified the SIESTA code and implemented the conductance eigenchannel analysis [25,29]. Fig. 3(a) presents the conductance–energy $G(E)$ curve for 3C-type (red line) at the Γ-point of 2D BZ (red dot) and the $G(E)$ curve for pristine GaAs nanowire without any structural defect (black line). Surprisingly, the electrical conductance does not drop at all within a large energy range from −1.7 eV to 0.8 eV. We chose two energy points for conductance eigenchannel analysis, 0.5 eV (blue dot) and −0.7 eV (green dot), where we found one and three eigenchannels, respectively. They are shown in Fig. 3(b) for 0.5 eV, and Fig. 3(c)–(e) for −0.7 eV. The red arrow indicated the position of 3C-type defect, which is basically a coherent twin boundary. All of them unambiguously show a direct turn of their wave functions at the twin boundary. More importantly, they all maintain a constant contour surface and perfect phase oscillation, indicating perfect electron transmission through these channels. Indeed, as shown in Fig. 3(b)–(e), the transmission coefficient T is almost unity.

However, as shown in Fig. 4(a), the above perfect transmission at Γ-point of 2D BZ does not happen at M-point (red dot) which is the middle point of zone boundary. Instead, electrical conductance (red line) at M has an extraordinary reduction across a large energy range from −1.7 eV to 1.7 eV. In this case, we also chose two energy points at 0.94 eV (blue dot) and 1.4 eV (green dot) for eigenchannel analysis where we found one and three eigenchannels, respectively. The channels are shown in Fig. 4(b)–(d). Different from the previous case, the twin boundary is no longer transparent for electrons at M point. The incoming electron wave packet from the bottom lead was strongly scattered by the twin boundary. Although the phase oscillation of electrons maintained after transmitted through the twin boundary, the magnitude of wave packet is reduced significantly, resulting in a reflection of wave function back to bottom lead. Consequently, the transmission coefficients of three eigenchannels decreases to 0.31, 0.86, and 0.15, shown in Fig. 4(b)–(d).

We have also performed the same analysis for GaAs with the 2AB-type defect, and observed a similar feature, that is, the conductance reduction at Γ point is much less than the reduction at M-point.

So the transmission coefficient T is found to be highly $\mathbf{k}_\perp$ dependent, where $\mathbf{k}_\perp$ is the in-plane wavevector $\perp$ ⟨1 1 1⟩. For coherent twin boundary (TB), $T(\mathbf{k}_\perp = 0) = 1$, which means the $\mathbf{k}_\perp = 0$ incoming waves do not even seem to notice the TB, and transmits right through as if the TB were transparent. This actually makes sense, in that, if one views the twinned nanowire purely edge-wise, and ignore in-plane displacement shifts – in effect collapsing all atoms edge-wise – one would not notice the presence of the TB. On the other hand, with larger $\mathbf{k}_\perp$, $T(\mathbf{k}_\perp)$ does drop significantly from 1. This agrees with our intuition that atomic-structure wise, the twin crystal presents a violent change of order, and can strongly scatter and scramble incoming waves.

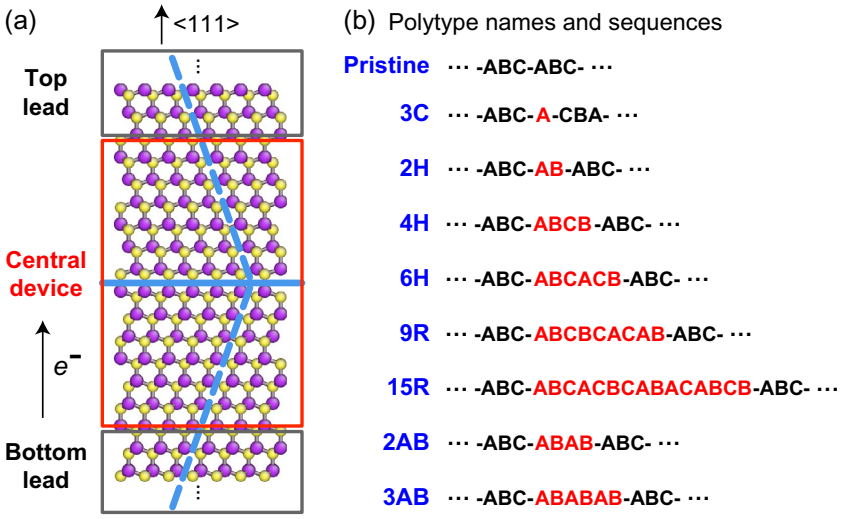

Fig. 1. (a) Simulation setup for quantum transport through GaAs⟨1 1 1⟩ nanowire with (b) nine representative polytypes of structural defects. Purple atoms: Ga; yellow atoms: As. (For interpretation of the references to colour in this figure legend, the reader is referred to the web version of this article.)

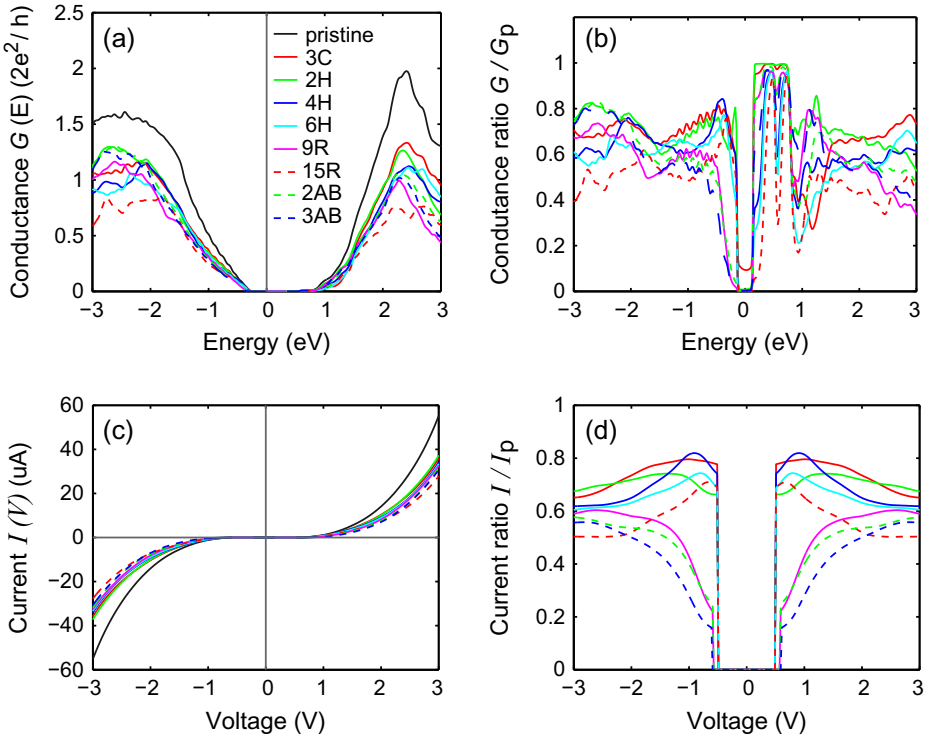

Fig. 2. Theoretical results of electrical conductance and current in GaAs⟨1 1 1⟩ nanowire with different polytypes of structural defects. (a) Total conductance–energy $G(E)$ curve. (b) Total conductance ratio with respect to pristine GaAs⟨1 1 1⟩ nanowire. (c) Total current–voltage $I(V)$ curve. (d) Total current ratio (I/I_p) with respect to the pristine nanowire.

3. Electron and hole mobilities in nanotwinned GaAs

The main question we ask about nanotwinned GaAs nanowires [35–37] (diameter 80 nm – 3 μm and long aspect ratios) is whether coherent twin boundaries (TB) are "strong" or "weak" scatterers of conduction electron and valence hole wavefunctions. In the limit that the TB is a 100% "strong" scatterer, like light scattering off a frosted glass, we may take $\lambda_{\mathrm{MFP}} = L_{\mathrm{TB}}$, where L_{TB} is the distance between two adjacent TBs. Then according to the classical Drude model, we should have

$$\sigma = e^2 L_{\mathrm{TB}} \left(\frac{c_{\mathrm{e}}}{\sqrt{m_{\mathrm{e}}^* k_{\mathrm{B}} T}} + \frac{c_{\mathrm{h}}}{\sqrt{m_{\mathrm{h}}^* k_{\mathrm{B}} T}} \right), \tag{3}$$

where $\sqrt{k_{\mathrm{B}} T / m^*}$ is the thermal velocity of carriers, following (2) and (1).

The assumption of "strong" scatterer, however, needs to be checked and verified by real calculations. Based on the quantum phase-coherent scattering calculations above, we can define a dimensionless scrambler strength:

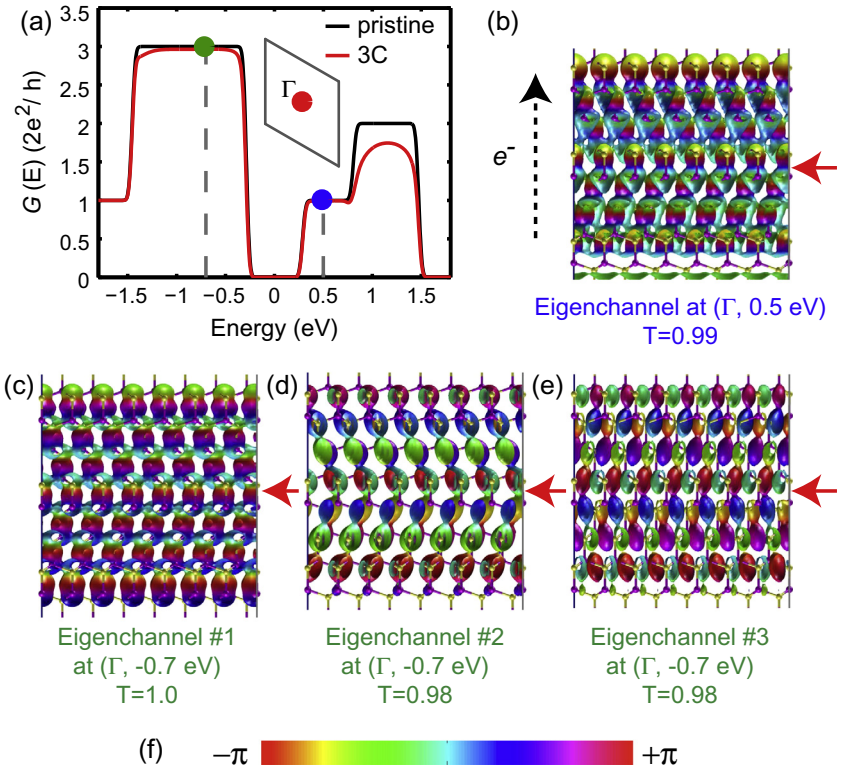

Fig. 3. Conductance analysis of 3C-type structural defect at Γ-point of 2D Brillouin zone perpendicular to the ⟨1 1 1⟩ direction. (a) Conductance–energy $G(E)$ curve at Γ-point. Black line: pristine GaAs⟨1 1 1⟩ nanowire; red line: GaAs⟨1 1 1⟩ nanowire with 3C-type structural defect. (b) Conductance eigenchannel at (Γ, 0.5 eV) marked as blue dot in (a). (c–e) Conductance eigenchannels at (Γ, −0.7 eV) marked as green dot. (f) Colormap of phase in the above real-space eigenchannels. (For interpretation of the references to colour in this figure legend, the reader is referred to the web version of this article.)

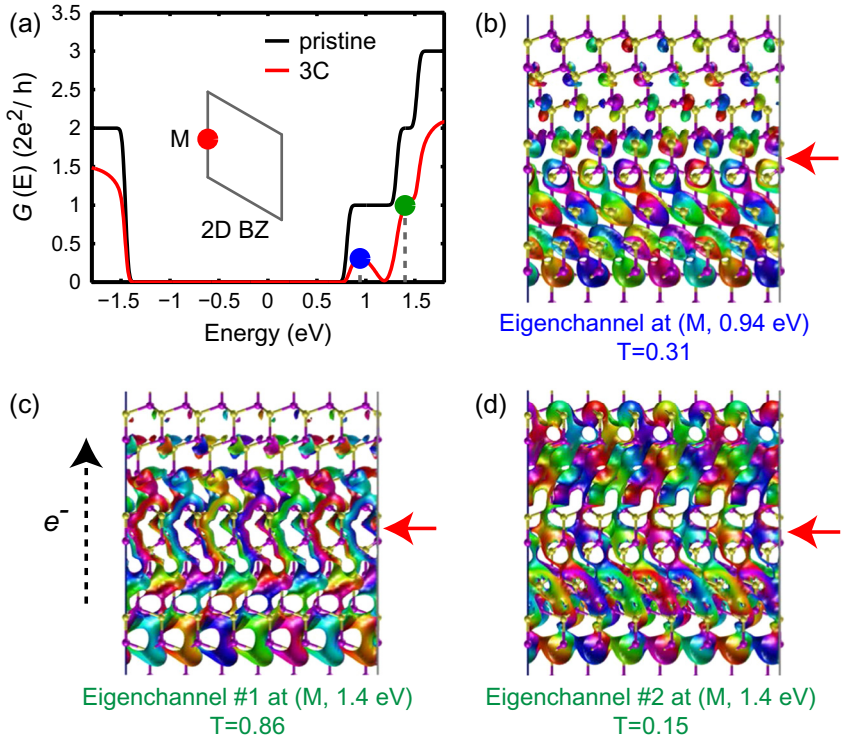

Fig. 4. Conductance analysis of 3C-type structural defect at M-point of 2D Brillouin zone perpendicular to the ⟨1 1 1⟩ direction. (a) Conductance–energy $G(E)$ curve at M-point. Black line: pristine GaAs⟨1 1 1⟩ nanowire; red line: GaAs⟨1 1 1⟩ nanowire with 3C-type structural defect. (b) Conductance eigenchannel at (M, 0.94 eV) marked as blue dot in (a). (c–e) Conductance eigenchannels at (M, 1.4 eV) marked as green dot. (For interpretation of the references to colour in this figure legend, the reader is referred to the web version of this article.)

$$s(\mathbf{k}_\perp,\varepsilon) \equiv 1-\frac{G(\mathbf{k}_\perp,\varepsilon)}{G_0(\mathbf{k}_\perp,\varepsilon)}, \tag{4}$$

where $\mathbf{k}_\perp=(k_x,k_y)$ labels the calculation where there could be a twin boundary in the z-direction, but periodic boundary condition in x and y are still maintained, so we can use (k_x,k_y) to label the pre- and post-transmission states. If there were no twin boundary, then the conductance would be

$$G_0(\mathbf{k}_\perp,\varepsilon)=n(\mathbf{k}_\perp,\varepsilon)\frac{2e^2}{h}, \tag{5}$$

where n is an integer: 0, 1, 2,..., to label the number of quantum channels with that $\mathbf{k}_\perp$ label and quasi-particle energy ε.

$G(\mathbf{k}_\perp,\varepsilon)$ is the same as $G_0(\mathbf{k}_\perp,\varepsilon)$, but with twin boundary structure "turned on". Thus, if $s=0$, we have perfect transmission and no loss ("weak" scatterer), while if $s=1$, we have very bad transmission and complete loss ("strong" scatterer) of momentum.

What was found, based on numerical calculations above, is that s is large for large $\mathbf{k}_\perp$'s. However, there is also a curious result that for $\mathbf{k}_\perp=0$,

$$s(\mathbf{k}_\perp=0,\varepsilon)=0, \tag{6}$$

What we need is then the thermally averaged scrambling strength for electrons:

$$\langle s_e\rangle=\frac{\sum_{\mathbf{k}_\perp}\int_\mu^{+\infty}d\varepsilon f(\varepsilon)G_0(\mathbf{k}_\perp,\varepsilon)s(\mathbf{k}_\perp,\varepsilon)}{\sum_{\mathbf{k}_\perp}\int_\mu^{+\infty}d\varepsilon f(\varepsilon)G_0(\mathbf{k}_\perp,\varepsilon)}, \tag{7}$$

that averages over existing electron states ($G_0(\mathbf{k}_\perp,\varepsilon)>0$), where $f_0(\varepsilon)$ is the Fermi–Dirac distribution:

$$f_0(\varepsilon) \equiv \frac{1}{e^{\frac{\varepsilon-\mu}{k_BT}}+1}, \tag{8}$$

and μ is the chemical potential of electrons, i.e. the Fermi level.

Similarly, for the hole states, we can define

$$\langle s_h\rangle=\frac{\sum_{\mathbf{k}_\perp}\int_{-\infty}^{\mu}d\varepsilon \bar{f}_0(\varepsilon)G_0(\mathbf{k}_\perp,\varepsilon)s(\mathbf{k}_\perp,\varepsilon)}{\sum_{\mathbf{k}_\perp}\int_{-\infty}^{\mu}d\varepsilon \bar{f}_0(\varepsilon)G_0(\mathbf{k}_\perp,\varepsilon)}, \tag{9}$$

where $\bar{f}_0(\varepsilon)$ is the hole concentration:

$$\bar{f}_0(\varepsilon) \equiv 1-f_0(\varepsilon)=\frac{1}{e^{\frac{\mu-\varepsilon}{k_BT}}+1}. \tag{10}$$

So, finally, we can semi-empircally correct (3) for variable-strength scattering as

$$\sigma=e^2L_{TB}\left(\frac{c_e}{\langle s_e\rangle\sqrt{m_e^*k_BT}}+\frac{c_h}{\langle s_h\rangle\sqrt{m_h^*k_BT}}\right). \tag{11}$$

with

$$M_e=\frac{eL_{TB}}{\langle s_e\rangle\sqrt{m_e^*k_BT}}, \quad M_h=\frac{eL_{TB}}{\langle s_h\rangle\sqrt{m_h^*k_BT}}. \tag{12}$$

Since we may not be dealing with intrinsic semiconductor, μ is not necessarily midway between valence band maximum (VBM) and conduction band minimum (CBM). The position of μ can influence $\langle s_e\rangle$ and $\langle s_h\rangle$. We can determine μ by experimental measurements of carrier concentrations, and knowing whether it is n-, p- or ambipolar type of conduction.

Calculations were performed for a long nanowire with averaged twin spacing of 2.42 nm. Due to the computation limit, we considered two sequences with twinned structures ("pristine-1–1–2–3–5-pristine", and "pristine-2–1–5–3–1-pristine"). The integer number in these two sequences indicates number of -ABC- or -CBA- segments, and twin boundary shows up between two adjacent segments by inserting an additional atomic layer. Moreover, we also considered the effect of the WZ phase by replacing single atomic layer at one of the six twin boundaries with an -AB- bilayer. In total, we therefore have 14 different configurations for transport calculations. The calculated scrambler strength factors are $\langle s_e\rangle=0.108\pm0.017$ and $\langle s_h\rangle=0.659\pm0.005$. Correspondingly, the estimated carrier mobilities are $M_e=3001.1\pm519.1\ cm^2/V/s$, and $M_h=477.2\pm5.2\ cm^2/V/s$, for μ midway between CBM and VBM. These values are in reasonable agreement with Ref. 17, indicating that the twin boundary in high density can lead to a significant reduction of electron and hole mobilities. The treatment above combines classical Drude model with quantum transmission coefficient calculations, which is related to but still different from Lee and Choi's approach based on the Boltzmann equation [38] when considering point-defect scatters in nanowires.

4. Summary

In summary, from first-principles DFT and Green's function method calculations, we found that the impact of twin boundaries and stacking faults on the electron transport in GaAs⟨1 1 1⟩ nanowire highly depends on specific polytype structure, energy-, and **k**-point in 2D BZ. Such strong dependence is a direct manifestation of quantum-interference effect. Our result shows that the conductance is reduced much more significantly in GaAs nanowires with WZ segment such as 2AB, 3AB, and 9R polytypes, which can be attributed to the larger band gap in the WZ phase than the ZB phase. In addition, conductance eigenchannel analysis allows the microscopic understanding of electron scattering at these planar defects. Finally, the carrier mobility calculated from a semi-empirical formula points out that the high-density twin boundaries can introduce significant reduction to electron and hole mobilities. For average twin spacing of 2.4 nm, electron mobility and hole mobility were predicted to be 3000 $cm^2/V/s$ and 500 $cm^2/V/s$, respectively. These findings highlight the necessity of removing twins and structural polytypes for high-performance nanowire solar cells.

Acknowledgment

This work was supported by Honda R&D Co., Ltd.

References

[1] J. Hu, T.W. Odom, C.M. Lieber, Acc. Chem. Res. 32 (1999) 435.
[2] M. Law, J. Goldberger, P. Yang, Annu. Rev. Mater. Res. 34 (2004) 83.
[3] Y. Li, F. Qian, J. Xiang, C.M. Lieber, Mater. Today 9 (2006) 18.
[4] R. Yan, D. Gargas, P. Yang, Nat. Photon. 3 (2009) 569.
[5] E.C. Garnett, M.L. Brongersma, Y. Cui, M.D. McGehee, Annu. Rev. Mater. Res. 41 (2011) 269.
[6] J.-C. Harmand, G. Patriarche, N. Péré-Laperne, M.N. Mérat-Combes, L. Travers, F. Glas, Appl. Phys. Lett. 87 (2005) 203101.
[7] J. Johansson, L.S. Karlsson, C.P.T. Svensson, T. Mårtensson, B.A. Wacaser, K. Deppert, L. Samuelson, W. Seifert, Nat. Mater. 5 (2006) 574.
[8] J. Johansson, L.S. Karlsson, C.P.T. Svensson, T. Mårtensson, B.A. Wacaser, K. Deppert, L. Samuelson, W. Seifert, J. Cryst. Growth 298 (2007) 635.
[9] L.S. Karlsson, K.A. Dick, J.B. Wagner, J.-O. Malm, K. Deppert, L. Samuelson, L.R. Wallenberg, Nanotechnology 18 (2007) 485717.
[10] C. Thelander, P. Caroff, S. Plissard, A.W. Dey, K.A. Dick, Nano Lett. 11 (2011) 2424.
[11] C.-Y. Yeh, Z.W. Lu, S. Froyen, A. Zunger, Phys. Rev. B 46 (1992) 10086.
[12] F. Glas, J. Appl. Phys. 104 (2008) 093520.
[13] A.X. Gray, C. Papp, S. Ueda, B. Balke, Y. Yamashita, L. Plucinski, J. Minár, J. Braun, E.R. Ylvisaker, C.M. Schneider, W.E. Pickett, H. Ebert, K. Kobayashi, C.S. Fadley, Nat. Mater. 10 (2011) 759.
[14] M. Murayama, T. Nakayama, Phys. Rev. B 49 (1994) 4710.
[15] Z. Zanolli, F. Fuchs, J. Furthmüller, U. von Barth, F. Bechstedt, Phys. Rev. B 75 (2007) 245121.
[16] F. Glas, J.-C. Harmand, G. Patriarche, Phys. Rev. Lett. 99 (2007) 146101.
[17] K. Shimamura, Z. Yuan, F. Shimojo, A. Nakano, Appl. Phys. Lett. 103 (2013) 022105.
[18] S.-P. Chiu, J.G. Lu, J.-J. Lin, Nanotechnology 24 (2013) 245203.

[19] C. Blömers, M.I. Lepsa, M. Luysberg, D. Grützmacher, H. Lüth, T. Schäpers, Nano Lett. 11 (2011) 3550.
[20] H. Yao, H. Günel, C. Blömers, K. Weis, J. Chi, J.G. Lu, J. Liu, D. Grützmacher, T. Schäpers, Appl. Phys. Lett. 101 (2012) 082103.
[21] D. Lucot, F. Jabeen, M.R. Ramdani, G. Patriarche, G. Faini, D. Mailly, J.-C. Harmand, J. Cryst. Growth 378 (2013) 546.
[22] S. Datta, Electronic Transport in Mesoscopic Systems, Cambridge University Press, 1997.
[23] M. Brandbyge, J.-L. Mozos, P. Ordejón, J. Taylor, K. Stokbro, Phys. Rev. B 65 (2002) 165401.
[24] X. Qian, J. Li, X. Lin, S. Yip, Phys. Rev. B 73 (2006) 035408.
[25] X. Qian, J. Li, S. Yip, Phys. Rev. B 82 (2010) 195442.
[26] P. Hohenberg, W. Kohn, Phys. Rev. 136 (1964) B864.
[27] W. Kohn, L.J. Sham, Phys. Rev. 140 (1965) A1133.
[28] J. Soler, E. Artacho, J.D. Gale, A. García, J. Junquera, P. Ordejón, D. Sánchez-Portal, J. Phys.: Condens. Matter 14 (2002) 2745.
[29] M. Paulsson, M. Brandbyge, Phys. Rev. B 76 (2007) 115117.
[30] D.C. Langreth, M.J. Mehl, Phys. Rev. B 28 (1983) 1809.
[31] A.D. Becke, Phys. Rev. A 38 (1988) 3098.
[32] J.P. Perdew, K. Burke, M. Ernzerhof, Phys. Rev. Lett. 77 (1996) 3865.
[33] N. Troullier, J. Martins, Phys. Rev. B 43 (1991) 1993.
[34] H.J. Monkhorst, J.D. Pack, Phys. Rev. B 13 (1976) 5188.
[35] J. Noborisaka, J. Motohisa, T. Fukui, Appl. Phys. Lett. 86 (2005) 213102.
[36] K. Ikejiri, J. Noborisaka, S. Hara, J. Motohisa, T. Fukui, J. Cryst. Growth 298 (2007) 616.
[37] H. Goto, K. Nosaki, K. Tomioka, S. Hara, K. Hiruma, J. Motohisa, T. Fukui, Appl. Phys. Exp. 2 (2009) 035004.
[38] H. Lee, H. Choi, Nano Lett. 10 (2010) 2207.